David Tomás Sánchez Martínez
Lourdes García Rodríguez
(coordinadores)

Proceedings of the 7th International Seminar on ORC Power Systems

Editorial Universidad de Sevilla

Proceedings of the 7th International Seminar on

ORC
Power Systems

David Tomás Sánchez Martínez
Lourdes García Rodríguez
(coordinadores)

Proceedings of the 7th International Seminar on

ORC Power Systems

(ORC2023)

4th to 6th
SEPTEMBER
SEVILLE 2023

EDITORIAL UNIVERSIDAD DE SEVILLA

Sevilla, 2024

Colección Actas
Núm.: 91

Review chairs of the 7th International Seminar on ORC Power Systems

Prof. Christoph Wieland (University of Duisburg-Essen) - *Review Chair*
Prof. Sotirios Karellas (National Technical University of Athens) - *Review Co-Chair*
Prof. Teemu Turunen-Saaresti (LUT University) - *Review Co-Chair*
Dr. Diego-César Alarcón-Padilla (Plataforma Solar de Almería - CIEMAT) - *Review Co-Chair*
Dr. Francesco Crespi (Universidad de Sevilla) - *Review Co-Chair*

ISBN 978-84-472-2745-7
DOI: https://dx.doi.org/10.12795/9788447227457

Diseño de cubierta y maquetación: los autores

INDEX OF CONTRIBUTIONS

DOI: https://dx.doi.org/10.12795/9788447227457_7

Performance analysis of a 1.5 MW organic Rankine cycle in a Carnot battery system for grid balancing services

Robin Tassenoy[1,*], Hannes Van De Velde[1], Kenny Couvreur[1], Michel De Paepe[1,2], Steven Lecompte[1,2]

[1]*Ghent University, Department of ElectroMechanical, Systems and Metal Engineering, Ghent, BE*
[2] *FlandersMake@UGENT, Core lab EEDT-MP, Leuven, BE*

*Corresponding Author: Robin.Tassenoy@UGent.be

ABSTRACT

Due to the increasing share of variable renewable energies in the energy mix, large-scale (>1 MW), long duration (>4 h) energy storage systems are becoming essential to ensure secure and stable energy supply. Carnot batteries, a combination of a power-to-heat, a thermal storage and a heat-to-power system, could provide a possible solution. Organic Rankine cycles have been considered as power-to-heat technology for Carnot batteries. However, it is not clear which grid services these organic Rankine cycles could deliver. To answer this question, a 1.5 MW organic Rankine cycle, suitable for integration in a Carnot battery, was modelled dynamically in Modelica. Dynamic finite volume heat exchanger models were used, while the operation of the pump and turbine was considered quasi-steady state due to their low time constant compared to the heat exchangers. The storage tanks were assumed perfectly mixed and modelled by time-varying boundary conditions. Furthermore, a control strategy driven by the requirements of the electrical grid was proposed. The dynamic model simulates and evaluates the organic Rankine cycles' response to the qualification test profiles for grid balancing services. It was found the organic Rankine cycle can deliver a 1 MW capacity for downward and upward secondary and tertiary reserve. Delivery of a 0.5 MW symmetric capacity for primary reserve is currently not possible due to the required full activation time. Nevertheless, the results indicate that the delivery of secondary and tertiary grid balancing services with the organic Rankine cycle could be an additional revenue stream to increase the financial feasibility of Carnot battery systems and it is thus worthwhile to investigate its potential financial benefits.

1 INTRODUCTION

1.1 Carnot batteries

Large deployment of variable renewable energies (VRE) challenges the stability of the electrical grid due to their intermittency. Energy storage can mitigate this problem by power and voltage smoothing, energy management, frequency regulation, peak shaving, load levelling, seasonal storage and standby generation during a fault (Argyrou et al., 2018). Therefore, energy storage is considered one of the main drivers to provide the flexibility needed to decarbonize the electricity grid.

The Carnot battery, a combination of a power-to-heat system, a thermal energy storage system (TES) and a heat-to-power system, is an emerging electrical energy storage concept that may provide additional flexibility to the grid. One of the Carnot battery's subsets is pumped thermal energy storage (PTES), in which an electrically driven heat pump is used to deliver heat to a hot store and/or extract heat from a cold store (McTigue et al., 2022). Organic Rankine cycles (ORCs) have been considered as heat-to-power system for Carnot batteries. Most studies have focused on the steady-state analysis and optimization of the storage concept and the obtainable round-trip efficiencies (Dumont et al., 2020). More recently, the techno-economic optimization of PTES has gained interest as well. Vecchi et al. (Vecchi et al., 2022) reviewed the techno-economic performance of Carnot batteries and discussed their applications at energy system scale. They showed Carnot batteries have been considered mainly for load-shifting and arbitraging services and concluded that these services alone may not be sufficient to recover the investment cost of the technology, highlighting the importance of a portfolio of grid services to provide different revenue streams.

1.2 Grid balancing services

Within the portfolio of grid services, providing grid flexibility is highly promising as the need intensifies due to the large deployment of VRE (Heggarty et al., 2019). Grid flexibility is usually defined as the possibility of modifying generation and/or consumption patterns in reaction to an external signal (e.g. price) to contribute to the power system stability in a cost-effective manner. At the transmission grid level, flexibility is linked to grid balancing services offered to transmission system operators (TSOs) (Villar et al., 2018). These services match the instantaneous electricity production and demand, which is essential to ensure stable grid operation. According to their time scale, three balancing products can be distinguished: primary or frequency containment reserve (FCR), secondary or automatically activated frequency restoration reserve (aFRR) and tertiary or manually activated frequency restoration reserve (mFRR). An overview of the main service characteristics is presented in Table 1.

Table 1: Characteristics of balancing services in the European electricity grid

Balancing service	Direction	Full activation time (FAT)	Min. delivery time	Min. bid size	Ref.
FCR	symmetric	30 s	15 min	1 MW	(Elia, 2019)
aFRR	up / down	7.5 min (to 5 min)	15 min	1 MW	(Elia, 2022a)
mFRR	up / down	15 min	15 min	1 MW	(Elia, 2022b)

1.3 Dynamic modelling ORC-based PTES with respect to grid balancing services

34

From the discussion above, it is clear that PTES dynamics are essential for the delivery of grid balancing services. However, there is a lack of research on these dynamic characteristics which makes it difficult to predict, regulate and optimize the performance of PTES in actual operation processes (Lu et al., 2022). While this knowledge gap has partially been addressed for Brayton-based PTES recently (Lu et al., 2022), literature discussing the dynamic behavior of ORC-based PTES is scarce.

Dynamic simulations of Rankine-based PTES are mostly focused on compressed heat energy storage systems, characterized by the use of latent thermal energy storage systems (Tafone et al., 2023). However, in these studies the ORC as a whole is modelled quasi-steady state. The dynamics of the ORC are thus completely neglected. To the best of the authors' knowledge, no study involving detailed dynamic modelling of a full Rankine-based grid-scale PTES is currently available.

Detailed dynamic simulation of large-scale ORC systems has been performed primarily in the context of waste heat recovery (Imran et al., 2020). Imran et al. (2020) stressed that profound understanding of the ORC dynamics is important for the development of controllers for ORC systems that encounter highly transient heat sources. Therefore, the ORC dynamics will also play a crucial role when evaluating the suitability of ORCs in PTES for grid balancing services, given the strict requirements on power response time and controllability, and the need to maintain suitable temperatures in the TES.

1.4 Scope of this study

No study discussing the dynamic response of a grid-scale Rankine-based PTES to grid requirements has been found. While the dynamic modelling and control of large-scale ORCs has been studied for waste heat recovery applications, similar studies have not been performed driven by the requirements for grid balancing services. In particular, there are no studies addressing this in the context of grid-scale Carnot batteries where, next to the strict requirements on power response time and controllability, also suitable TES temperatures need to be maintained. This study aims at making a first step towards assessing Rankine-based PTES for delivery of grid balancing services by focusing on the ORC subsystem. A dynamic model of a 1.5 MW ORC suitable for implementation in PTES was constructed. Then, a suitable control strategy was developed to follow the desired power production, while maintaining correct TES temperatures. Finally, the technical potential to deliver grid balancing services was assessed by validation of the controlled system against the prequalification tests of the European grid.

2 METHODOLOGY

2.1 Carnot battery lay-out and heat pump boundary conditions

This work focusses on the dynamic modelling of an ORC to be implemented in a Carnot battery. These PTES systems usually consist of a vapor compression heat pump, a TES and an ORC, as shown in Figure 1. This topology has been chosen over an alternative configuration using a single thermal machine as compressor (during charging) and expander (during discharging) or sharing heat exchangers between both operation modes. Although such systems have a lower investment cost, they are currently less mature and limited to smaller system sizes (Dumont et al., 2020).

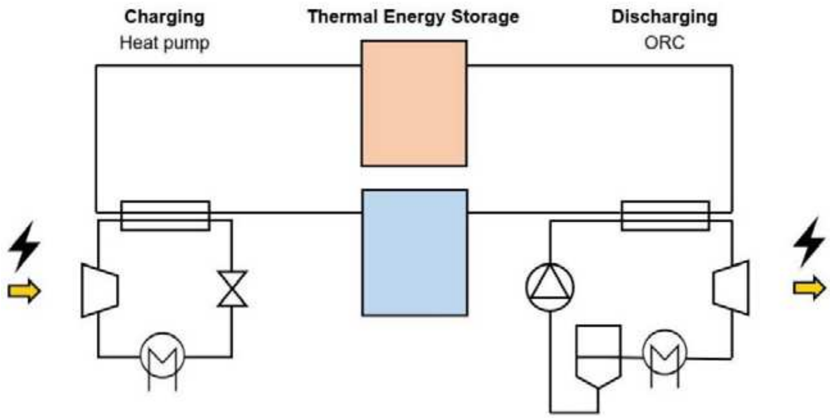

Figure 1: Schematic representation of a Rankine-based, thermally integrated Carnot battery

35

Rankine-based PTES typically takes advantage of a low-grade heat source to boost the electric round-trip efficiency of the system (Frate et al., 2017). Apart from low grade geothermal heat and solar thermal energy, heat sources of suitable thermal capacity and temperature level can be found mostly in the industrial sector. Balancing the heat availability and efficiency improvement of the PTES, a residual heat source of 65 °C was assumed for heat pump integration (Marina et al., 2021). As typical temperature lifts of heat pumps range from 40 to 80 °C (Arpagaus et al., 2018), the TES temperatures have been chosen to fit this range. Sensible liquid heat storage is often applied as it is reliable, mature and cost-efficient. A two-tank configuration guarantees almost constant charge and discharge profiles and was therefore selected instead of a single tank solution, despite the cost of doubling the storage volume (Frate et al., 2017). Pressurized water tanks were opted for as they are cheap, have low environmental impact and are suitable for the temperature range of interest (Dumont et al., 2020). It was assumed the water enters the ORC evaporator at 120 °C, while it returns to the cold tank at 95 °C. The ORC heat sink was assumed to be water with a constant inlet temperature of 15 °C. R1233zd(E) was selected as working fluid from a list of refrigerants suitable for ORCs in the intended operating range (De Paepe et al., 2019), considering thermodynamic and environmental performance.

As shown in Figure 1, the basic ORC system considered in this work has five main components: the pump, evaporator, turbine, condenser and liquid receiver. Although more complex topologies with higher efficiencies have been proposed in literature (Lecompte et al., 2015), the additional components increase the thermal inertia of the system and are thus expected to slow down the system's dynamic response. Therefore, the basic system was assessed first. If this topology proves suitable to deliver grid balancing services, more complex topologies can be addressed in future work.

2.2 Nominal operating conditions

A steady-state ORC model was developed in Python 3.7.9 to determine the nominal operating conditions of the different components. The fluid properties of R1233zd(E) were retrieved from REFPROP (Eric W. Lemmon, 2018). An overview of the main modelling assumptions and resulting nominal conditions is given in Table 2.

Table 2: Nominal operating conditions: modelling assumptions and results

Assumed parameter	Value	Unit	Output parameter	Value	Unit
$T_{water,ev,in}$	120	°C	$p_{evaporator}$	10.4	bar
$T_{water,ev,out}$	95	°C	$p_{condenser}$	1.7	bar
$T_{water,cond,in}$	15	°C	$pressure\ ratio$	6.29	-
$PP_{evaporator}$	5	°C	$\dot{m}_{water,ev}$	109.83	kg/s
$PP_{condensor}$	5	°C	$\dot{m}_{water,cond}$	179.81	kg/s
$SH_{evaporator}$	5	°C	$\dot{m}_{refrigerant}$	47.59	kg/s
$SC_{condenser}$	3	°C	$\dot{Q}_{evaporator}$	11.4	MW
$\eta_{is,pump}$	70	-	$\dot{Q}_{condenser}$	9.9	MW
$\eta_{is,turbine}$	87.23	-	η_{cycle}	12.8	%
$P_{el,turbine}$	1.5	MW			

2.3 Component selection and modelling

Based on the results of the steady-state cycle calculation, suitable components were selected. A dynamic ORC model was built in the object-oriented modelling language Modelica (The Modelica Association, 2023), using the simulation software Dymola 2022 (AB, 2021) and the TIL-library (TLK Thermo GmbH & IfT 2020). The component models of this library were used, and extended when necessary. Fluid properties were calculated using REFPROP (Eric W. Lemmon, 2018). 36

Plate heat exchangers (PHE) were selected for both the evaporator and condenser because they are relatively cheap, compact and have a modular design (Imran et al., 2020). Funke (Funke, 2022) produces gasketed PHE with capacities up to 30 MW and volume flow rates up to 4500 m³/h. The stainless steel FP 405 and FP 41 gasketed PHE were selected as evaporator and condenser. The PHE were modelled using the finite volume (FV) model available in the TIL-library, assuming countercurrent flow. The suitability of FV-models for dynamic simulation of evaporators and condensers has extensively been demonstrated (Imran et al., 2020). Moreover, the PHE-model of the TIL-library was successfully used to simulate dynamic behavior of PHE before (Meesenburg et al., 2020). The plate dimensions of the Funke heat exchangers were used as model input. The inside geometry of the heat exchangers was not made public by the manufacturer. Therefore, the inside geometry proposed by Lee et al. (Lee et al., 2018) and Zhang et al. (Zhang et al., 2019) were used for the evaporator and condenser respectively. The pressure drop correlation proposed by Zhang et al. (Zhang et al., 2019) was used in the condenser. The pressure drop correlation by Lee et al. (Lee et al., 2018) was initially used in the evaporator. Using this correlation required a very high number of calculation cells in the heat exchanger to avoid numerical fluctuations. Therefore, the refrigerant pressure drop correlation in the evaporator was simplified and assumed quadratic to the mass flow (Meesenburg et al., 2020). Although this simplification slightly affects the numerical values of the resulting evaporator pressure, it does not directly affects the heat exchanger dynamics. As the current study focusses on this dynamic response, this simplification was found to be acceptable. For the refrigerant side, following heat transfer correlations have been added to the TIL-library: Chisholm and Wanniarachchi (García-Cascales et al., 2007) for single-phase flow, Desideri et al. (Desideri et al., 2017) for evaporation and Zhang et al. (Zhang et al., 2019) for condensation. Heat transfer at the water side was modelled by the VDI Plate alpha correlation (Holger, 2010) available in the TIL-library.

Both the pump and expander were modelled quasi-steady state, which means part-load performance was taken into account and an immediate response of the components was assumed. These assumptions are commonly made when dynamically modelling ORCs (Imran et al., 2020). A variable turbopump was modelled by the *pump2ndOrder* – model of the TIL-library with nominal pressure difference equal to 10.5 bar and nominal volume flow rate equal to 328.2 m^3/h at a nominal rotational speed of 48.3 Hz. The *EffExpander*-model from the TIL-library was extended to a performance map based model. Performance maps detailing the relation between refrigerant mass flow rate and turbine isentropic efficiency, pressure ratio and rotational speed were used to determine the turbine operating point. Currently, the turbine was modelled based on the performance map of a two-stage axial turbine NASA-CR-168289 (Timko, 1984). This high-pressure turbine is typically used in aeronautic applications. If more appropriate data for refrigerant turbines becomes available, this data can be implemented in the performance map based model. In this study the original map was rescaled using dynamic similitude to the nominal operating conditions, which was considered acceptable as the current study focusses on the dynamic performance.

A liquid receiver was added to absorb the working fluid fluctuations during operation and ensure liquid state at the pump inlet (Andritos et al., 2016). The receiver was modelled using the TIL-model. The sensible storage was not modelled in detail. Instead, a two-tank system with two perfectly mixed tanks was assumed. The water temperature at the inlet of the evaporator was thus assumed constant. A boundary model was used to impose a constant inlet temperature and pressure, while the water mass flow could be regulated.

2.4 Control strategy

The control system should make sure the ORC quickly delivers the required power production, while maximizing operational efficiency and maintaining correct TES temperatures. Therefore, three inputs were controlled using PI-controllers: the pump rotational speed, the turbine rotational speed and the water mass flow rate in the evaporator. Variable speed control of the pump is an effective way of controlling the refrigerant mass flow and consequently, the expander power. As the operating point is determined by the intersection of the pump- and expander characteristic, the expander speed was varied as function of the pressure ratio to maximize the turbine efficiency. Finally, the water mass flow in the evaporator was adapted by the PI-controller to maintain a cold storage supply temperature of 95 °C. All PI-constants were determined by analyzing the corresponding system step response in Python 3.7.9. The resulting PI-constants are summarized in Table 3. 37

Table 3: PI-control parameters

Controller	**k [-]**	k_i $[s^{-1}]$
Pump	1.55e-6	4.16e-6
Turbine	1343	1680
Water mass flow	1.16	4.44

2.5 Test conditions for grid balancing services

The Belgian TSO, Elia, provides prequalification tests for all balancing services discussed in Table 1. The power profiles evaluate the full activation time (FAT), the maximum power delivery, the duration of the service and the power deviation. The delivery of FCR is always symmetric and the capacity should react linearly to the frequency deviation of the grid. aFRR and mFRR on the other hand can deliver down- or up regulation separately, or do both. It should be noted that Elia sets the minimum capacity bid at 1 MW, but it is allowed to split this capacity over multiple assets. The main criterium is that the requested power uptake or production (within predefined accuracy) is reached within the prescribed FAT. In this study, the combination of down- and up regulation was not tested as it follows from the separate tests. The ORC was tested for a 1 MW capacity for mFRR and aFRR in the downward and upward direction and for a 0.5 MW symmetric FCR capacity. The prequalification tests also aim at verifying that the service can be delivered for a sufficiently long time. For Carnot batteries, this duration is closely related with the capacity and state-of-charge of the TES. Here, focus was given to the reaction time and it was assumed the TES was sized adequately, fulfilling the duration requirement.

3 RESULTS AND DISCUSSION

3.1 Steady – state model validation

A direct validation of the different component models to experimental data is not possible, as this data is not available. Instead, the component sizing and modelling are partly validated by comparison of the steady-state results to the steady-state python calculation. The dynamic model (and implemented control) are tested by simulating the steady-state system response to constant controller setpoints. An overview of the assumed boundary conditions, controller setpoints and corresponding simulation results is given in Table 4. The deviation can be explained by the model strategy. While the thermodynamic states are fixed directly in the Python model, they follow from the physical component characteristics and choice of controlled parameters in the Modelica model. A one-on-one match is thus not to be expected. Nevertheless, the good correspondence between the results indicates proper sizing and modelling of the different components. Moreover, the controllers reach the desired setpoints illustrating the effectiveness of the implemented control method.

Table 4: Steady-state model validation: boundary conditions and simulation results

Assumed parameter	Value	Unit	Output variable	Value	Unit
$T_{water,ev,in}$	120	°C	$T_{water,ev,out}$	95	°C
$T_{water,cond,in}$	15	°C	$P_{el,turbine}$	1.5	MW
$T_{water,ev,out,set}$	95	°C	$p_{evaporator}$	9.2	bar
$P_{el,turbine,set}$	1.5	MW	$p_{condenser}$	1.6	bar
$\dot{m}_{water,cond,in}$	180	kg/s	$pressure\ ratio$	5.7	[-]
Output variable	**Value**	**Unit**	$\dot{Q}_{evaporator}$	12.2	MW
$\dot{m}_{water,ev}$	115.4	kg/s	$\dot{Q}_{condenser}$	10.7	MW
$\dot{m}_{refrigerant}$	47.4	kg/s	η_{cycle}	12.3	%

3.2 Ramping test

All grid balancing services require a sufficiently low FAT, implying the full offered capacity should be activated within this time period. The required FATs are summarized in Table 1. The prequalification test of FCR and aFRR includes a ramping test, in which the desired power is ramped between the capacity limits over the full allowable FAT. The maximum allowable deviation during the ramp is prescribed. For mFRR, the ramp itself is not prescribed. The prequalification test just requires activation within 15 minutes. Therefore, a ramp of 10 minutes was applied and the maximum power deviation after 15 minutes from the start of the activation was verified. In Figure 2, the result of the ramping test for the delivery of a 0.5 MW FCR capacity is shown. The ramping tests for a 1 MW aFRR and mFRR are analogous but ramp between 0.5 and 1.5 MW instead of the symmetric capacity shown for FCR. A summary of the simulated deviations and the allowable tolerance is given in Table 5. As can be seen, the power response for mFRR and aFRR is suitable, while the power deviation exceeds the allowable margin for FCR. In Figure 2, it can be seen that the power production slightly lags the desired setpoint. This deviation is more pronounced in the upward direction than in the downward direction. In both cases, the actual ramping rate is too slow to remain within the allowable tolerance of 10 %.

Table 5: Results of the ramping tests

Service	Maximum measured deviation [%]	Allowable tolerance [%]
mFRR down / up	0	/
aFRR (down and up)	1.5	7.5
FCR	19.2	10

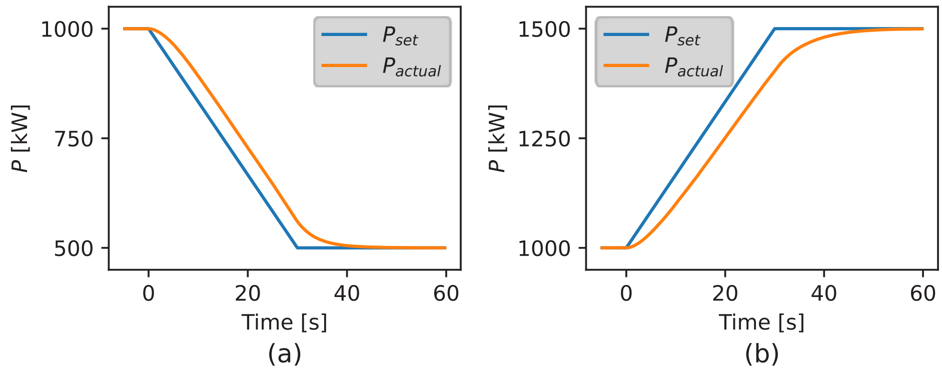

Figure 2: Ramping test for 0.5 MW symmetric FCR capacity: (a) downward and (b) upward ramp

During this modulation, the return temperature to the cold TES tank should remain correct to conclude the Carnot battery satisfies the FAT criterium of the grid services. In Figure 3, the variation of the water temperature at the outlet of the evaporator is shown for the downward and upward FCR ramp, respectively. For the downward ramp, the maximum absolute temperature deviation equals 0.08 °C. The maximum deviation during the upward step is even smaller and equals 0.05 °C. As expected, the largest temperature deviations occur during the fastest ramps. The maximum deviations during the aFRR and mFRR tests are even smaller. Moreover, the deviations are of short duration. Therefore, the return temperatures are acceptable for all steps.

The FAT requirement is thus fulfilled for a 1 MW mFRR and aFRR capacity in the downward and upward direction. The FAT requirement for FCR is not fulfilled due to limitations on the system's maximum ramping rate.

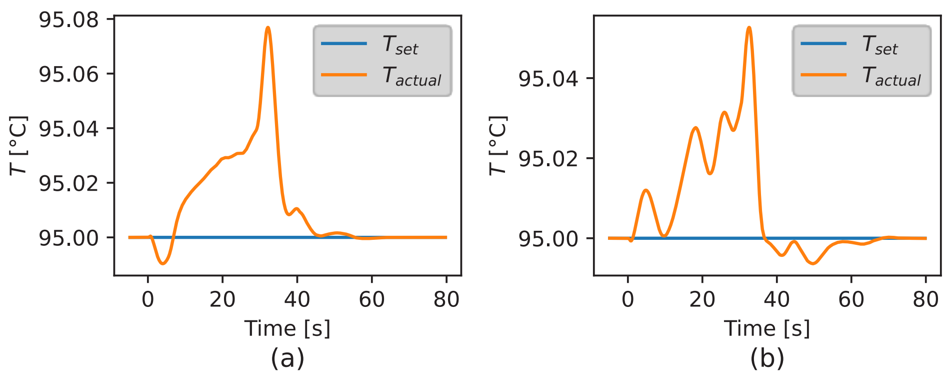

Figure 3: Water temperature at the evaporator outlet during the ramping test for 0.5 MW symmetric FCR capacity: (a) downward and (b) upward ramp

3.3 Tertiary reserve

Next to the duration requirement, the delivery of tertiary reserve is only determined by the FAT requirement discussed in Section 3.1. The ORC can thus deliver a 1 MW mFRR capacity in both the downward and upward direction.

3.4 Secondary reserve

As discussed in Section 3.1, the ORC meets the FAT requirement for aFRR. Next to this requirement, the ORC should be able to follow a synthetic load pattern within a margin of 7.5 %. A maximum of 30 deviations outside this margin is allowed. The aFRR load-following test is illustrated in Figure 4. The average absolute deviation is 0.86 and 0.78 % for the downward and upward product respectively. The maximum absolute deviation of the upward product is 1.50 %, which is below the allowed margin. The downward test shows some unexpected peaks, which are due to numerical reasons. Significantly increasing the number of calculation cells in the evaporator eliminates these numerical fluctuations.

However, as this also significantly increases calculation time, this has been verified for the downward part of the load-following test only and the full test (including the numerical fluctuations) is shown here. Numerical fluctuations occur at four separate moments. The 7.5 % margin is exceeded at only two of these (20 timesteps on a total of 18457), which is within the 30 allowed deviations. During the test, the maximum absolute deviations of the water temperature at the evaporator outlet are 1.25 and 0.02 °C for the downward and upward test. The ORC thus qualifies for an aFRR capacity of 1 MW in both directions.

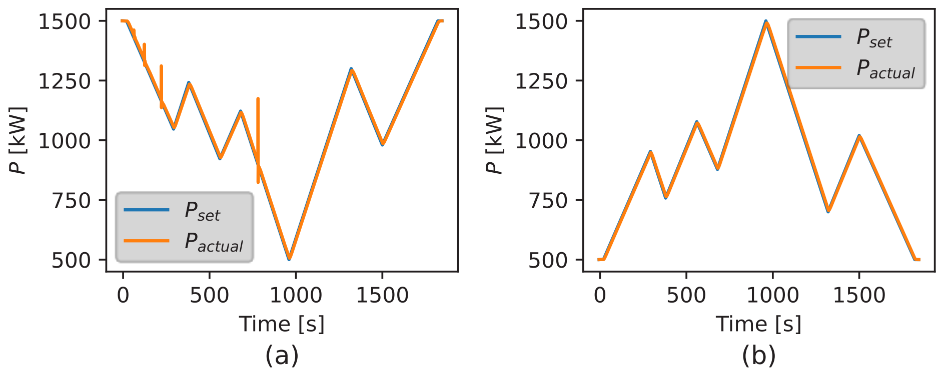

Figure 4: Load-following test for the (a) downward and (b) upward aFRR-product

3.5 Primary reserve

As discussed in Section 3.1 the FAT requirement for FCR is currently not met, due to the maximum ramping rate found with the current control mechanism. Besides this FAT criterium, the system should pass a linearity check by reacting suitably to step changes of one fourth of the contracted capacity. The required FCR capacity should be delivered within a 10 % tolerance margin 12.5 s after the step. The maximum relative deviation values per step are summarized in Table 6. All deviations are within the allowable tolerance. The maximum absolute deviation of the water temperature at the evaporator outlet over the whole ramping interval is 1.24 and 0.22 °C for the stepwise decrease and increase in turbine power output. Although the linearity check is fulfilled, the system currently thus not qualifies for a 0.5 MW symmetric FCR capacity due to the FAT requirement. 40

Table 6: Overview of power deviations in FCR prequalification test

	Downward FCR		Upward FCR	
Step	P_{set} **[kW]**	**Max deviation [%]**	P_{set} **[kW]**	**Max deviation [%]**
1	875	0.85	1125	6.55
2	750	1.91	1250	3.98
3	625	1.21	1375	3.30
4	500	1.01	1500	3.48

4 CONCLUSIONS

The possibility to deliver grid balancing services with large-scale ORCs in Rankine-based Carnot batteries was investigated. Therefore, a Rankine-based 1.5 MW ORC, suitable for implementation in a Carnot battery using two-tank liquid storage, was modelled dynamically in Modelica. Afterwards, a suitable system control strategy was developed and the system was evaluated according to the prequalification tests for grid balancing services in the European grid. Under the assumption of quasi-steady state thermal machine modelling and ideal behavior of the sensible storage tanks, the system can deliver a capacity of 1 MW for aFRR and mFRR, both in the downward and upward direction. A symmetric capacity of 0.5 MW for FCR is currently not possible due to limitations on the maximum ramping rate of the system. Further research on dynamic ORC control to improve the system's maximum ramping rate would thus be valuable. The results indicate that the delivery of secondary and tertiary balancing services with the ORC could be another revenue stream to increase the financial feasibility of Carnot battery systems and it is thus worthwhile to investigate the potential financial benefits. In future work, the dynamic model will be extended to a full dynamic Carnot battery model including detailed modelling of the TES and heat pump cycle, hence further investigating optimal system scheduling within the energy system.

NOMENCLATURE

η	efficiency	
aFRR	automatically activated frequency restoration reserve / secondary reserve	(-)
FAT	full activation time	(s)
FCR	frequency containment reserve / primary reserve	(-)
$\dot{m}$	mass flow rate	(kg/s)
mFRR	manually activated frequency restoration reserve / tertiary reserve	(-)
ORC	organic Rankine cycle	(-)
p	pressure	
P	power	
PHE	plate heat exchanger	
PP	pinch point	
PTES	pumped thermal energy storage	(-)
$\dot{Q}$	heat transfer rate	(-)
SC	subooling	(K)
SH	superheat	(K)
T	temperature	
TES	thermal energy storage	(-)
TSO	transmission system operator	(-)
VRE	variable renewable energies	(-)

Subscript

cond	condenser
el	electrical
ev	evaporator
in	inlet
is	isentropic
out	outlet
set	setpoint

REFERENCES

AB, D. S. 2021. Dymola - Dynamic Modelling Laboratory - Full User Manual. In

Andritos, G., Desideri, A., Gantiez, C., Lemort, V., & Quoilin, S. 2016. Steady state and dynamic modelling of a 1 MWel commercial waste heat recovery ORC power plant *29th International conference on Efficiency, Cost, Optimisation, Simulation and Environmental Impact of Energy Systems*, Slovenia.

Argyrou, M. C., Christodoulides, P., & Kalogirou, S. A., 2018, Energy storage for electricity generation and related processes: Technologies appraisal and grid scale applications, *Renewable and Sustainable Energy Reviews*, *94*: p. 804-821.

Arpagaus, C., Bless, F., Uhlmann, M., Schiffmann, J., & Bertsch, S. S., 2018, High temperature heat pumps: Market overview, state of the art, research status, refrigerants, and application potentials, *Energy*, *152*: p. 985-1010.

De Paepe, M., Lecompte, S., & Pillai, A. 2019. CHESTER D3.4 - Detailed design of the ORC laboratory prototype.

Desideri, A., Zhang, J., Kærn, M. R., Ommen, T. S., Wronski, J., Lemort, V., & Haglind, F., 2017, An experimental analysis of flow boiling and pressure drop in a brazed plate heat exchanger for organic Rankine cycle power systems, *International Journal of Heat and Mass Transfer*, *113*: p. 6-21.

Dumont, O., Frate, G. F., Pillai, A., Lecompte, S., De paepe, M., & Lemort, V., 2020, Carnot battery technology: A state-of-the-art review, *Journal of Energy Storage*, *32*: 101756.
Elia. 2019. FCR service design note.
Elia. 2022a. Automatic Frequency Restoration Process (aFRR/R2). Retrieved 06/11/2022 from https://www.elia.be/en/electricity-market-and-system/system-services/keeping-the-balance/afrr
Elia. 2022b. Balancing services: mFRR - design note.
Eric W. Lemmon, I. H. B., Marcia L. Huber, Mark O. McLinden. 2018. REFPROP Documentation, Release 10.0.
Frate, G. F., Antonelli, M., & Desideri, U., 2017, A novel Pumped Thermal Electricity Storage (PTES) system with thermal integration, *Applied Thermal Engineering*, *121*: p. 1051-1058.
Funke. 2022. PLATE HEAT EXCHANGERS - Variety and top product quality.
García-Cascales, J. R., Vera-García, F., Corberán-Salvador, J. M., & Gonzálvez-Maciá, J., 2007, Assessment of boiling and condensation heat transfer correlations in the modelling of plate heat exchangers, *International Journal of Refrigeration*, *30*(6): p. 1029-1041.
Heggarty, T., Bourmaud, J.-Y., Girard, R., & Kariniotakis, G., 2019, Multi-temporal assessment of power system flexibility requirement, *Applied Energy*, *238*: p. 1327-1336.
Holger, M. 2010. Pressure Drop and Heat Transfer in Plate Heat Exchangers.
Imran, M., Pili, R., Usman, M., & Haglind, F., 2020, Dynamic modeling and control strategies of organic Rankine cycle systems: Methods and challenges, *Applied Energy*, *276*: 115537.
Lecompte, S., Huisseune, H., van den Broek, M., Vanslambrouck, B., & De Paepe, M., 2015, Review of organic Rankine cycle (ORC) architectures for waste heat recovery, *Renewable and Sustainable Energy Reviews*, *47*: p. 448-461.
Lee, D., Kim, D., Park, S., Lim, J., & Kim, Y., 2018, Evaporation heat transfer coefficient and pressure drop of R-1233zd(E) in a brazed plate heat exchanger, *Applied Thermal Engineering*, *130*: p. 1147-1155.
Lu, C., Shi, X., He, Q., Liu, Y., An, X., Cui, S., & Du, D., 2022, Dynamic modeling and numerical investigation of novel pumped thermal electricity storage system during startup process, *Journal of Energy Storage*, *55*: 105409. 42

Marina, A., Spoelstra, S., Zondag, H. A., & Wemmers, A. K., 2021, An estimation of the European industrial heat pump market potential, *Renewable and Sustainable Energy Reviews*, *139*: 110545.
McTigue, J. D., Farres-Antunez, P., J, K. S., Markides, C. N., & White, A. J., 2022, Techno-economic analysis of recuperated Joule-Brayton pumped thermal energy storage, *Energy Conversion and Management*, *252*: 115016.
Meesenburg, W., Markussen, W. B., Ommen, T., & Elmegaard, B., 2020, Optimizing control of two-stage ammonia heat pump for fast regulation of power uptake, *Applied Energy*, *271*: 115126.
Tafone, A., Pili, R., Pihl Andersen, M., & Romagnoli, A., 2023, Dynamic modelling of a compressed heat energy storage (CHEST) system integrated with a cascaded phase change materials thermal energy storage, *Applied Thermal Engineering*, *226*: 120256.
The Modelica Association. 2023. https://modelica.org/index.html
Timko, L. P. 1984. Energy efficient engine: high pressure turbine component test performance report (NASA contractor report; 162829, Issue.
TLK Thermo GmbH & IfT 2020. TIL 3.7 – Model library for thermal components and systems. In
Vecchi, A., Knobloch, K., Liang, T., Kildahl, H., Sciacovelli, A., Engelbrecht, K., Li, Y., & Ding, Y., 2022, Carnot Battery development: A review on system performance, applications and commercial state-of-the-art, *Journal of Energy Storage*, *55*: 105782.
Villar, J., Bessa, R., & Matos, M., 2018, Flexibility products and markets: Literature review, *Electric Power Systems Research*, *154*: p. 329-340.
Zhang, J., Kærn, M. R., Ommen, T., Elmegaard, B., & Haglind, F., 2019, Condensation heat transfer and pressure drop characteristics of R134a, R1234ze(E), R245fa and R1233zd(E) in a plate heat exchanger, *International Journal of Heat and Mass Transfer*, *128*: p. 136-149.

This book contains the compilation of works contributed to the *7th International Seminar on Organic Rankine Cycle Power Systems* (ORC 2023), held in Seville between the 4th and 6th of September 2023. The event was hosted by Universidad de Sevilla on behalf of the Knowledge Centre on Organic Rankine Cycle Technology (KCORC), incorporated in The Netherlands.

The ORC conference, organized biennially, stems as the only conference that is specific to ORC technology, therefore gathering a diverse community whose affiliation spans across all the interested stakeholders, not only in this particular technology but also and in a broader context, in the energy transition. Original equipment manufacturers, professional associations, end-users, investors, policy makers, academics, scientists feel at home at ORC 2023.

The almost 100 proceedings in this book cover a wide variety of topics, from fundamentals to system integration through component design, accounting for thermodynamic performance as well as component design. In addition to this, and as a new track in 2023, works on heat pump technology were also accepted in order to raise awareness of the strong ties between both technologies, specifically in energy storage applications.

This book provides an excellent overview of the current maturity of power systems based on Organic Rankine Cycle technology for applications as diverse as geothermal and waste heat recovery in industry or downstream of other prime movers (e.g., marine applications). It is also an excellent source of information to understand the current challenges faced by the technology, stemming from a very competitive market and increasingly stringent environmental regulations.

The organizers of ORC 2023 hope that the reader finds this work as exciting as the attendees to the conference and, maybe, make the decision to join the 8th edition to the conference in 2025.

KCORC
KNOWLEDGE CENTER
ORGANIC RANKINE CYCLE

eUS EDITORIAL
UNIVERSIDAD DE SEVILLA